Internal curing by superabsorbent polymers in alkali-activated slag

Li, Zhenming; Wyrzykowski, Mateusz; Dong, Hua; Granja, José; Azenha, Miguel; Lura, Pietro; Ye, Guang

DOI
10.1016/j.cemconres.2020.106123

Publication date
2020

Document Version
Final published version

Published in
Cement and Concrete Research

Cement and Concrete Research 135 (2020) 106123

Contents lists available at ScienceDirect

Cement and Concrete Research

journal homepage: www.elsevier.com/locate/cemconres

Internal curing by superabsorbent polymers in alkali-activated slag

Zhenming Li[a,*], Mateusz Wyrzykowski[b], Hua Dong[a], José Granja[c], Miguel Azenha[c], Pietro Lura[b,d], Guang Ye[a,e]

[a] Department of Materials and Environment (Microlab), Faculty of Civil Engineering and Geoscience, Delft University of Technology, Delft, the Netherlands
[b] Empa, Swiss Federal Laboratories for Materials Science and Technology, Dübendorf, Switzerland
[c] ISISE, Department of Civil Engineering, School of Engineering, University of Minho, Guimarães, Portugal
[d] Institute for Building Materials, ETH Zurich, Zurich, Switzerland
[e] Magnel Laboratory for Concrete Research, Department of Structural Engineering, Ghent University, Ghent, Belgium

ARTICLE INFO

Keywords:
Alkali-activated slag
Shrinkage
Cracking
Superabsorbent polymers
Mechanical properties

ABSTRACT

In this study, internal curing by superabsorbent polymers (SAP) is utilized to mitigate self-desiccation and autogenous shrinkage of alkali-activated slag (AAS) pastes. Absorption and desorption kinetics of SAP incorporated in AAS pastes were studied with X-ray tomography. Internal curing delayed the peak of the rate of heat liberation but increased the total reaction degree of AAS pastes. Internal curing by SAP mitigated effectively the drop of internal relative humidity and the self-desiccation-induced autogenous shrinkage of AAS pastes. The cracking tendency of AAS pastes undergoing shrinkage in restrained conditions was also significantly reduced with SAP. Nonetheless, adding SAP, regardless of their content, cannot eliminate the autogenous shrinkage of AAS pastes, suggesting the existence of other autogenous shrinkage mechanism(s) besides self-desiccation.

1. Introduction

Slag based alkali-activated materials have emerged as eco-friendly alternatives to binders based on ordinary Portland cement (OPC) [1]. Compared to Portland cement, alkali-activated slag (AAS) entails around 25–50% lower CO_2 emissions and more than 40% lower embodied energy in the production process [2,3]. AAS is typically prepared by mixing alkali solution with ground granulated blast-furnace slag, a by-product of the iron ore smelting industry [4]. When used as a binder material, AAS shows high strength, good chemical resistance and fire resistance [5–7]. However, several drawbacks of AAS, such as fast setting and large shrinkage, limit a wide application of this material in engineering [8,9]. It has been reported in the literature that mixtures based on AAS can exhibit several times higher autogenous shrinkage than mixtures based on OPC [10]. The high autogenous shrinkage of AAS can increase the cracking potential of the concrete [11].

Many studies have been conducted to mitigate the autogenous shrinkage of AAS, e.g. [12–18]. Palacios and Puertas [12] found that a shrinkage reducing admixture (SRA) made from polypropylene glycol can reduce the autogenous shrinkage of AAS mortar. SRA made from polyethylene glycol with high molecular weight shows similar effects [19]. However, it should be noted that admixtures that are intensively used in OPC-based systems may be ineffective in alkali-activated materials [20–22]. For example, CaO as an expansive agent can compensate the shrinkage of OPC [23], but in AAS system CaO was found to increase the shrinkage by refining the pore structure [15]. Gypsum, as another example, can increase the amount of expansive phases formed in AAS at early age, but the consequent expansion was not sufficient to compensate for the long-term shrinkage [15]. Ye and Radlińska [15] and Bakharev et al. [24] reported that curing the samples at 60–80 °C before demoulding was effective in reducing the subsequent drying shrinkage of AAS systems. This method may also work in mitigating the autogenous shrinkage, since the deformability of the C-A-S-H gels was reported to be reduced at elevated temperature curing [15]. Nonetheless, high-temperature curing is generally unsuitable for cast-in-situ concrete. Sakulich and Bentz [13] showed that internal curing by prewetted lightweight aggregate mitigated the autogenous shrinkage of AAS mortar. Furthermore, Oh and Choi [17] and Song et al. [18] found that using superabsorbent polymers (SAP) as internal curing agents also led to lower autogenous shrinkage of AAS mortar. Tu et al. [25] reported that internal curing by SAP was effective in mitigating the autogenous shrinkage of alkali-activated fly ash-slag paste.

In fact, internal curing by SAP has been widely reported to have beneficial effects on mitigating the self-desiccation and the consequent autogenous shrinkage of Portland cement and blast-furnace slag cement [26–31]. In AAS systems, self-desiccation is also an important

* Corresponding author.
E-mail address: z.li-2@tudelft.nl (Z. Li).

https://doi.org/10.1016/j.cemconres.2020.106123
Received 27 January 2020; Received in revised form 16 May 2020; Accepted 26 May 2020

mechanism of autogenous shrinkage according to Li et al. [10] and Ye and Radlińska [14]. Therefore, SAP would be expected to reduce also the autogenous shrinkage of AAS. Despite this potential and the preliminary results reported in [13,17,18,25], studies in this field are still limited. For example, the absorption of SAP in alkali solution and the shrinkage-mitigating mechanism of SAP in AAS are not well understood. Besides, no results on the impact of internal curing by means of SAP on the self-induced stress and on the cracking tendency of AAS under restrained conditions have been reported so far.

This study aims at exploring the effectiveness of internal curing by SAP in mitigating the autogenous shrinkage and the early-age cracking of AAS. The absorption capacity of SAP in alkali solutions was first measured with the teabag method [32] and the dosage of SAP in AAS pastes was designed accordingly. The influence of internal curing on the reaction kinetics was examined through isothermal calorimetry. X-ray tomography was utilized to track the liquid desorption from the SAP and the microstructure of the SAP-containing mixtures. The internal relative humidity evolution, the autogenous deformation (corrugated tube method) and the self-induced stress (restrained ring tests) of the plain AAS and internally cured pastes were studied. At last, the compressive strength and Young's modulus of AAS pastes were measured.

2. Materials and methods

2.1. Materials

The precursor was ground granulated blast-furnace slag (hereinafter-termed slag) from Ecocem Benelux. The chemical composition of the slag is given in Table 1. The loss of ignition of the slag was determined according to ASTM D7348–08. The density of the slag was 2.89 g/cm^3. The particle size range, determined by laser diffraction, was 0.1–50 μm, with a d_{50} of 18.3 μm.

The activator was a combination of sodium hydroxide, sodium silicate and deionized water at mass ratio 1:7.25:6.25. The concentrations of Na_2O and SiO_2 in the activator were 9.5 mass-% (corresponding to 3.8 M) and 13.8 mass-% (correspond to 2.9 M), respectively. The pH of the activator was obtained from the OH^- concentration (titration method) as 14.6. After mixing, the solution was allowed to cool for 24 h before mixing with the precursor and dry SAP. The density of the alkaline activator was 1.23 g/cm^3.

The SAP used were based on a cross-linked copolymer of acrylamide and acrylate obtained in bulk polymerization and were anionic. The SAP had particles of irregular shape and sizes up to 500 μm, with a dominant size around 200 μm, see Fig. 1. No SAP degradation (dissolution) was evident during the teabag tests in the activator (the activator remained clear without any traces of SAP leaching out and there was no self-release of the absorbed fluid).

2.2. Determination of SAP content

2.2.1. Absorption capacity of SAP

The absorption capacity of SAP in the activator ($NaOH/Na_2SiO_3$ solution) was measured by the teabag method according to [33]. To understand better the absorption behavior of the SAP in different solutions, the absorption capacities of the SAP in deionized water and NaOH solution were also measured. The NaOH solution had the same Na_2O/H_2O ratio as the activator. To measure the free absorption potential, 0.2 g of dry SAP particles were inserted in each teabag. Three

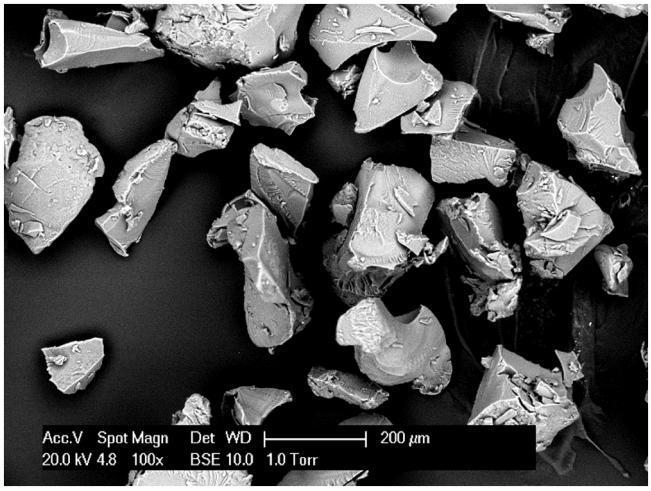

Fig. 1. Scanning Electron Microscopy image of dry SAP particles.

individual teabags were prepared for each solution to ensure the reliability of the results. The teabag containing the SAP was hung in a beaker filled with the fluid (about 100 ml). The beaker was tightly covered with a paraffin stretch film to avoid carbonation and evaporation of the fluid. After 15 min, 30 min, 60 min, 3 h and 24 h of contact time, the teabag (with the hydrogel inside) was removed and weighed. The detailed testing procedure and formulas used to calculate the absorption capacity can be found in [32]. Considering the fast setting of the AAS pastes, the absorption capacity in the activator at 3 h, equal to 20 g/g, was used to calculate the necessary amount of dry SAP.

It should be noted that in an AAS paste, Ca^{2+} also exists in the initial pore solution of the paste and may influence the actual absorption capacity of SAP as reported e.g. in [34,35]. In addition, the ions concentrations in the pore solution can change with time. Therefore, the absorption capacity of the SAP in the activator may be different from that in the AAS paste. In order to take those effects into account, the initial pore solution of the paste before the SAP complete the absorption process, instead of the activator, should be used for the absorption capacity test. However, it is difficult to obtain pore solution from the paste in the first hours after casting by the hydraulic piston method, since the paste has not obtained enough stiffness yet (the stiffness evolution will be discussed in detail in Section 4.3). In this case, a slurry of paste instead of fluid will be obtained by hydraulic pressing. Moreover, due to the fast setting of the paste (around 0.5 h, as will be shown in Section 3.3), the release of Ca^{2+} from the dissolution of slag and the changes in the concentrations of ions are supposed to be limited by the time the SAP cavities have formed [36,37]. Therefore, the activator instead of the actual pore solution of the paste was used to measure the absorption capacity of the SAP.

To investigate whether the SAP preferentially absorb ions or water when they are immersed in the activator, 0.4 g of SAP (which were expected to absorb about 8 g of solution) were put into 20 g of activator and the concentrations of the ions in the activator before and after SAP absorption were measured. 20 g was chosen because the amount of solution should be as low as possible to magnify the possible influence of SAP absorption on the concentrations of the ions of the surrounding solution, but in the meantime, the solution should be enough to submerge the SAP during absorption. Three individual solutions and

Table 1
Chemical compositions of slag.

Oxide (wt%)	CaO	Al_2O_3	SiO_2	MgO	Fe_2O_3	TiO_2	SO_3	K_2O	MnO	Other	L.o.I.
Slag	40.50	13.25	31.77	9.27	0.52	0.97	1.49	0.34	0.36	0.21	1.31

L.o.I.: loss on ignition.

teabags were prepared for each absorption time (30 min, 60 min, 3 h and 24 h). After absorbing for a given time, the teabag with the SAP was taken out, and the ions concentrations of the solution left were measured. The concentration of OH^- was measured by titration against diluted HCl acid solution (0.1 mol/l). Phenolphthalein was used as the indicator. The elemental concentrations of Na and Si were measured by a PerkinElmer Optima 5300 DV ICP-OES (Inductively Coupled Plasma Optical Emission Spectrometry). The average values of three replicates are presented.

2.2.2. SAP content design

In order to prevent self-desiccation, the amount of liquid absorbed by the SAP should compensate for the chemical shrinkage of a binder [35]. This approach was assumed here also for the AAS binder. The desired liquid/binder ratio provided by the SAP (l/b_{SAP}) can be calculated by Eq. (1):

$$l/b_{SAP} = \mathrm{CS}\cdot\alpha_{max}\cdot\rho_a \quad (1)$$

where CS [cm^3/g] is the chemical shrinkage of the paste, α_{max} [-] is the estimated maximum degree of reaction of the paste, ρ_a [g/cm^3] is the density of the activator.

Since there has been no theoretical ultimate chemical shrinkage of AAS reported in the literature, the measured chemical shrinkage of AAS until the age of 28 days, 0.042 ml/g, is used here to replace the product $CS \cdot \alpha_{max}$. The chemical shrinkage of the AAS paste was measured by dilatometry according to ASTM C 1608 [38], only the water was replaced by the activator to be added onto the surface of the paste [39]. ρ_a is 1.23 g/cm^3 as measured by pycnometry [40]. Accordingly, l/b_{SAP} is calculated to be 0.052.

The amount of SAP to be added to the precursor, m_{SAP} [g], is determined according to the absorption capacity, AC, of the SAP in the activator (emulating the initial pore solution absorbed by the SAP during mixing) and the desired amount of the internal curing liquid, $l/b_{SAP} \cdot m_{binder}$:

$$m_{SAP} = \frac{l/b_{SAP}\cdot m_{binder}}{\mathrm{AC}} \quad (2)$$

Accordingly, the desired amount of SAP was calculated to be 0.26% by mass of the binder (slag).

2.3. Mixtures

The liquid/binder ratio (l/b) of the plain AAS paste was 0.5 (the control mixture). The l/b in the internally cured AAS paste was designed so that the *basic* l/b (corresponding to the liquid not absorbed by the SAP) was the same. The total l/b of the internally cured AAS paste was therefore the sum of the basic l/b and l/b_{SAP} = 0.5 + 0.052 = 0.552. Additionally, higher amounts of SAP (0.5% and 1%) and correspondingly higher amounts of internal curing activator were also applied (it was assumed that the SAP absorb the same amount of activator, 20 g/g, in mixtures with higher l/b). The goal was to obtain a maximal autogenous shrinkage reduction and a minimal strength reduction. For each total l/b, a mixture without SAP was also tested as reference. All mixtures compositions are shown in Table 2. A 5-l Hobart mixer was used for making the paste. After premixing of the precursor with the dry SAP for 1 min, the activator was added during low-speed mixing. The mixing continued at low speed for 1 min and for another 2 min at high speed.

2.4. Reaction heat

A TAM Air-314 isothermal calorimeter (Thermometric) was used to measure the reaction heat of AAS pastes. The temperature of the measuring channels of the calorimeter was controlled at 20 ± 0.01 °C. Approximately 5 g of paste was cast into glass vials (internal diameter 24.5 mm) and the vials were immediately loaded into the measuring chambers. The mixing and loading procedures lasted about 15 min from the moment of adding activator. The heat flow data were recorded every minute until 7 days. The reaction heat results are normalized by the weight of slag.

2.5. Times of initial and final set

The times of initial and final set were measured by an automatic Vicat machine. Plastic films were used to cover the samples during the measurements to avoid the influence of evaporation on the setting time of the pastes [29].

2.6. Internal relative humidity

The internal relative humidity (RH) in AAS pastes was measured with Rotronic DT stations equipped with HC2-AW water activity probes. Miniature (few grams) specimens were put directly after mixing in hermetic chambers (Ø43mm × 12 mm) and the water activity probes were located above them (at a distance of about 15 mm). In these setups, the volume of the specimen is similar to the volume of air above it and hence the RH measured in the latter is dominated by that of the specimen.

Two replicates were measured for each material. The probes have a nominal accuracy of ± 1% RH. Before and after each measurement, calibration was performed on each probe with four saturated salt solutions (NaCl, KCl, KNO_3 and K_2SO_4) in the range 75–98% RH. The data were recorded at 1-min intervals for 7 days.

To account for the influence of dissolved ions on the internal RH, the RH of the pore solution of the pastes cured for 9 h, 1, 3 and 7 days was also measured. The pore solution was extracted from the paste by a steel die under high pressure and the RH measurement followed the same procedure as for the pastes.

The RH depression due to curvature effect of the menisci can be approximated according to Eq. (3) [41].

$$RH = RH_S RH_K \quad (3)$$

where RH is the (measured) internal RH of the paste, RH_S is due to the presence of dissolved species and RH_K is due to curvature effects.

2.7. Linear autogenous shrinkage

Corrugated tubes with a length of 425 mm and an external diameter of 28.5 mm were utilized to measure the linear autogenous shrinkage of AAS pastes [42]. Three replicates were measured for each mixture. The length changes were automatically measured by linear variable differential transformers (LVDTs) until 7 days. The measuring bench together with the samples was immersed in a silicone oil bath with temperature controlled at 20 ± 0.1 °C. A detailed description of the method can be

Table 2
Mixture compositions (by mass proportion) of AAS pastes with and without SAP.

Mixtures	AAS0.5	AAS0.552	AAS0.552SAP	AAS0.6	AAS0.6SAP	AAS0.7	AAS0.7SAP
Slag	1	1	1	1	1	1	1
Activator	0.5	0.552	0.552	0.6	0.6	0.7	0.7
SAP	–	–	0.0026	–	0.005	–	0.01

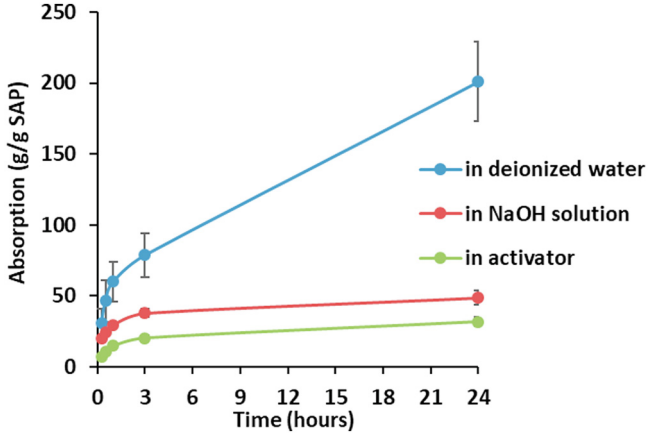

Fig. 2. Absorptions of SAP in deionized water, NaOH solution and activator measured with the teabag method.

found in [43]. The strains were referenced to the length of the sample at final set determined by Vicat needle in parallel tests, where the samples were protected from evaporation by means of a plastic film. A low scatter of the calculated strains (1–2%) was observed for the parallel samples after final set.

2.8. Self-induced stress

The stress induced by restrained autogenous shrinkage in AAS pastes with and without SAP was characterized by the dual ring test [44,45]. In this test, the pastes were poured in between two concentrically placed steel rings to form a paste ring. While the sides of the paste ring were sealed by the adjacent steel rings, its upper surface was covered with polyethylene foil fixed with adhesive aluminum tape to avoid evaporation. The maximum stress in the paste due to shrinkage restrained by the inner ring was calculated as [46]:

$$\sigma_{max} = -\varepsilon \cdot E \cdot \left(\frac{R_{IP}^2 - R_{II}^2}{2R_{IP}^2}\right)\left(\frac{R_{OP}^2 + R_{IP}^2}{R_{OP}^2 - R_{IP}^2}\right) \quad (4)$$

where σ_{max} is the maximum stress in the paste ring; ε is the measured strain of the inner ring; E is the elastic modulus of the ring; R_{II}, R_{IP}, and R_{OP} are the inner radius of the restraining ring (75 mm), the inner radius (87.5 mm) and outer radius of the paste ring (125 mm), respectively.

2.9. X-ray micro computed tomography

To investigate the absorption and desorption behaviors of SAP in AAS paste, the mixture AAS0.552SAP was scanned with X-ray tomography using a Micro-CT-Scanner (Phoenix Nanotom). The paste was first cast into a small plastic container with diameter of 4 mm and height of 6 mm. Immediately after casting, the container was sealed by paraffin film and put into the CT scanner. During the first week after casting, the same sample was scanned 4 times, at the age of 1 h (nominally, in reality starting immediately after mixing), 8 h, 1 day and 7 days, respectively. The X-ray source tube worked at 120 kev/60 mA. 1900 images were acquired on a digital GE DXR detector (2304 × 2304 pixels). The duration of each scan was 1 h. The reconstructed dataset had a voxel size of 5 μm. The 3D Reconstruction of the slices was carried out with VG Studio Max.

2.10. Mechanical properties

The compressive strength of AAS pastes with different l/b and different amounts of SAP was measured at the curing age of 14 h and 6 days according to NEN-196-1 [47]. The Young's modulus was measured automatically through EMM-ARM (which stands for 'Elasticity Modulus Monitoring through Ambient Response Method') [48] from about 20 min after casting until 7 days at 10 min intervals. This method is based on measuring vibrations of a composite beam made of a hollow acrylic tube (internal diameter 16 mm, wall thickness 2 mm) filled with fresh paste. The beam is fixed at one end in a massive steel frame and hence forms a 450-mm long cantilever. A miniature accelerometer is mounted on the free end and the vibrations of the beam are enhanced throughout the measurement by a room ventilator located at a distance of about 0.5 m from the test setup. From the accelerations of the free end of the composite beam, the first resonant frequency is determined. The latter is used to estimate the Young's modulus of the beam. The detailed measuring procedure is reported in [48].

3. Results

3.1. Absorption behaviors of SAP

The time-resolved free (teabag) absorption curve of the SAP in the activator within 24 h is shown in Fig. 2. For comparison, the absorption curves in NaOH solution and deionized water are also shown in Fig. 2. The absorption capacity of the SAP in the AAS paste was assumed to correspond to the absorption in the activator at 3 h, 20 g/g. As mentioned in Section 2.2.1, this value was used to calculate the amount of SAP in the mix design of the internally cured mixtures.

To investigate whether the composition of the solution absorbed by the SAP is different from that of the surrounding activator, the ions concentrations in the activator before and after exposure to the SAP were measured. As shown in Fig. 3, the concentrations of Na, Si, and OH^- of the activator change little (within 3.5%) after absorption by SAP for different lengths of time. The changes are in particular evident at the longest exposure time, 24 h. Even though the changes were statistically significant according to analysis of variance (ANOVA) at 0.01 significance level, it should be noted that the changes presented here are amplified by the high amount of SAP relative to the amount of pore solution (in fact, about 40% of all available solution was absorbed by the SAP). In the real paste, the amount of solution is considerably higher (only about 10% of the solution is absorbed in the paste with 0.552 l/b), hence the changes in the concentration of ions would be about 4 times less significant, likely below 1%. That allows assuming that the SAP absorb the alkali solution approximately as a whole and the preference for certain ions during absorption can be in first approximation neglected in the paste.

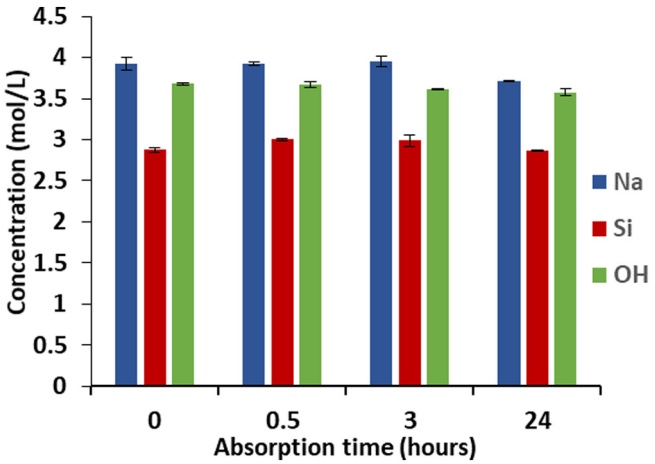

Fig. 3. Concentrations of Na, Si and OH^- in activator before (0 h) and after (0.5, 3 and 24 h) absorption by SAP.

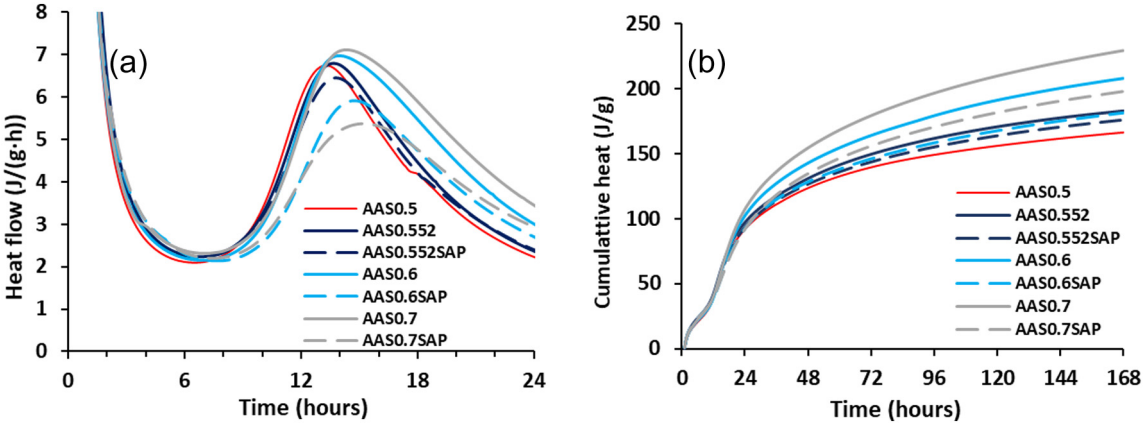

Fig. 4. Heat flow (a) and cumulative heat (b) of AAS pastes with different l/b and different amounts of SAP (see Table 2).

3.2. Reaction heat

The heat release results of AAS pastes with and without SAP are shown in Fig. 4. The pastes show dormant periods of around 8–9 h, dependent on the l/b and the presence of SAP. The main reaction peak occurs between 13 and 15 h. The main heat release peaks appear later as l/b increases from 0.5 to 0.7 when SAP is not incorporated. In the meantime, the main peak becomes broader. When the SAP are incorporated, the main peaks appear later and show lower amplitudes for the samples with the same total l/b. The dormant period also becomes slightly longer for SAP-containing mixtures, especially for AAS0.6SAP and AAS0.7SAP, whose liquid contents are much higher than the control mixture AAS0.5. The decrease of the reaction rate after the main peak is normally attributed to the inhibited dissolution of the precursor because of the continuous formation of reaction products surrounding slag and the gradually blocked pore space [62].

As shown in Fig. 4(b), the control paste AAS0.5 shows the lowest cumulative heat. The cumulative heat increases with increasing l/b, and the pastes without SAP generate more hydration heat than the pastes with SAP and the same l/b. The latter effect is more significant at higher l/b (for 0.552, the paste without SAP releases only slightly more heat than the one with SAP). All pastes, with and without SAP, generate very similar cumulative heat in the first 12 h. After that time, the differences among the curves become more and more evident.

3.3. Setting time

The times of initial and final set are shown in Table 3. The initial and final set occur later for the pastes with higher l/b without SAP. However, for pastes with SAP, the time of initial set is similar to the control mixture AAS0.5, which is likely due to the similar basic l/b of these mixtures. The times of final set of SAP-containing pastes are longer than for the control mixture but shorter than for the non-SAP mixtures with the same total l/b.

Table 3
Times of initial and final set of AAS pastes with and without SAP.

Mixtures	Initial set (min)	Final set (min)
AAS0.5	25	35
AAS0.552	36	51
AAS0.552SAP	24	39
AAS0.6	40	65
AAS0.6SAP	25	56
AAS0.7	55	80
AAS0.7SAP	35	70

3.4. Internal RH

The internal *RH* evolution in the control mixture AAS0.5 and in the internally cured mixture AAS0.552SAP are presented in Fig. 5. The measured RH_S of the pore solutions of the mixtures and the calculated RH_K due to the curvature effect are also shown in Fig. 5. Since the RH_S due to the dissolved ions could not be monitored continuously, the interpolated values of the experimental RH_S results were used to calculate the RH_K. The RH_K values in the first hour (which are calculated as slightly higher than 100%) and the fluctuation of the RH_K curve for AAS0.552SAP at around 3 days probably originate from the cumulative experimental errors during the measurement of both *RH* and RH_S.

It can be seen from Fig. 5 that *RH* and RH_S of the two mixtures increase in the first 8–9 h, which is most likely caused by the decrease of ion concentrations during the dissolution of slag and the formation of initial reaction products [37,49]. In fact, the RH_S is approximately linearly proportional to the molar proportion of water in the pore fluid [50]. This relationship has been recently used in [49] to follow the reaction kinetics of fly ash-based geopolymers.

After the initial increase, the RH_S of the two mixtures stabilize at around 95%. Meanwhile, the AAS0.5 undergoes a severe drop in RH_K, indicating the occurrence of self-desiccation. Internal curing by 0.26% SAP (AAS0.552SAP) keeps the RH_K of the paste close to 100% until a slight decrease occurs at around 150 h. This indicates that the self-desiccation in the AAS paste is mitigated by the addition of 0.26% SAP.

3.5. Autogenous shrinkage

Fig. 6 shows the linear autogenous shrinkage of the plain and internally cured AAS pastes in the first week of reaction. To investigate the influence of higher SAP contents, the autogenous shrinkage of mixtures with 0.5% and 1% of SAP and correspondingly higher l/b (see Table 1) are also shown in Fig. 6.

The shrinkage of the control mixture AAS0.5 develops rapidly after final set time, reaching over 3600 μm/m at 1 day and around 6600 μm/m at 7 days. Increasing the liquid content without adding SAP reduces the autogenous shrinkage only slightly. By adding 0.26 mass-% SAP, the autogenous shrinkage is drastically reduced, reaching only about 1800 μm/m at 1 day and 2760 μm/m at 7 days. The relative reductions at 1 day and 7 days are 51% and 58%, respectively. These values are similar to the ones for AAS mortar reported in [17,18], which were around 50% on the first day and 66% at 180 h. Increasing the SAP dosage (together with the corresponding absorbed liquid amount) to 0.5% or 1%, however, does not lead to any significant change in the measured shrinkage.

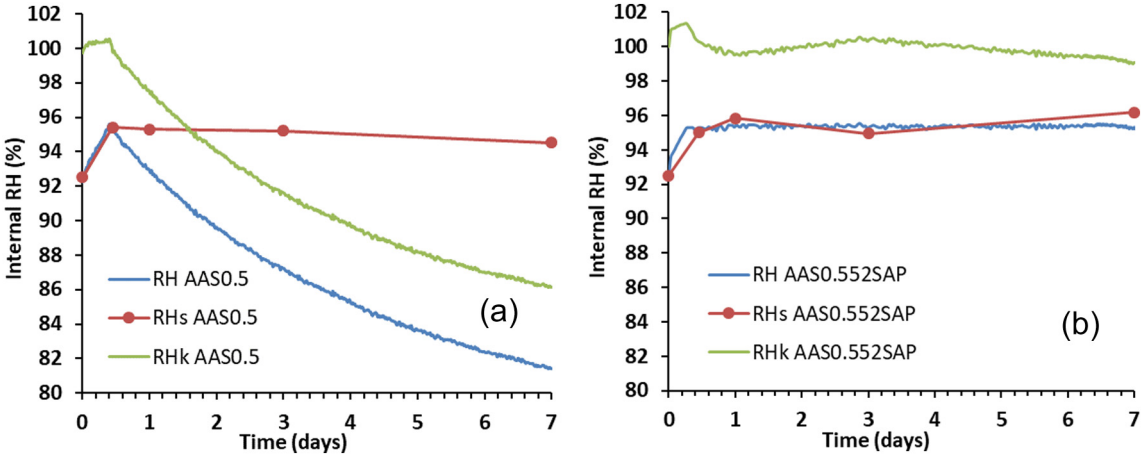

Fig. 5. Internal RH results of AAS0.5 (a) and AAS0.552SAP (b). The RH of the pastes was measured continuously while the RH_S of the pore solutions of the pastes was measured at individual curing ages of 0 h, 9 h, 1, 3 and 7 days. The RH_k was calculated with Eq. (3).

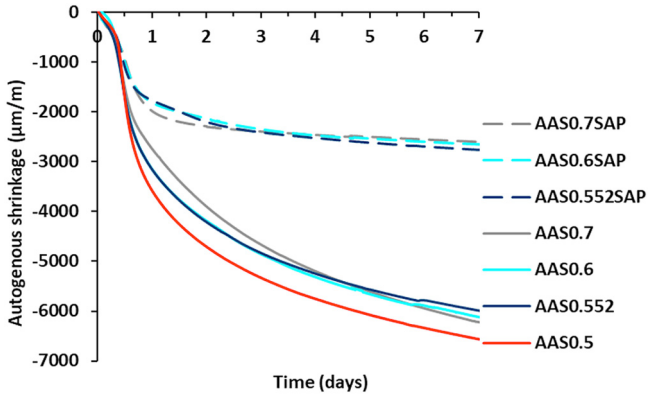

Fig. 6. Autogenous shrinkage of AAS pastes with different l/b and different amounts of SAP. The strains are referenced to the length at final set.

3.6. Self-induced stress and cracking

The self-induced stress developments in AAS0.5, AAS0.552, and AAS0.552SAP measured with the dual rings are shown in Fig. 7(a). A zoom into the period within the first 24 h is shown in Fig. 7(b). Mixtures with higher amounts of SAP than 0.26% were not measured, since they did not show significantly different autogenous shrinkage (see Fig. 6).

In the first 8–9 h, which correspond to the dormant period indicated by the heat flow (see Fig. 4), the three mixtures all generate stress close to zero. After this period, the stresses in mixtures without SAP develop rapidly and each experiences a sudden drop after several hours, which indicates through cracking in the paste ring. AAS0.5 cracks at 12.3 h with the stress reaching 2.7 MPa, while the cracking of AAS.552 occurs about half an hour later, with the stress reaching 2.2 MPa. This indicates a lower tensile strength of the mixture with higher liquid content. The stress in AAS0.552SAP also increases after the dormant period but at a much lower rate. Cracking in the internally cured paste did not happen until around 5 days, when the stress reached 4.4 MPa. The results show that internal curing by SAP greatly reduced the rate of stress evolution and postponed the cracking time of the paste, a result that cannot be achieved by just increasing the liquid l/b [29].

3.7. X-ray micro-computed tomography analysis

A representative horizontal cross-section of AAS0.552SAP specimen at different time points obtained from an X-ray microtomography 3-D dataset (tomogram) is shown in Fig. 8. Based on the grey levels, several phases can be distinguished within the paste (light grey in general), including unreacted slag particles (white), SAP with liquid (dark grey), entrapped air (black and spherical) and newly formed voids/pores (black, marked by the arrows) within the SAP-originated voids.

Fig. 8(a) shows in the paste the randomly distributed swollen SAP particles, indicating that the SAP absorbed liquid before solidification of the paste. The size of the SAP after absorption can reach more than 0.5 mm. At the age of 8 h (Fig. 8(b)), voids are already formed within the cavities originally occupied by the swollen SAP, confirming the liquid release from SAP to the surrounding paste, i.e. internal curing. At the age of 1 day, the volume of newly formed voids increases,

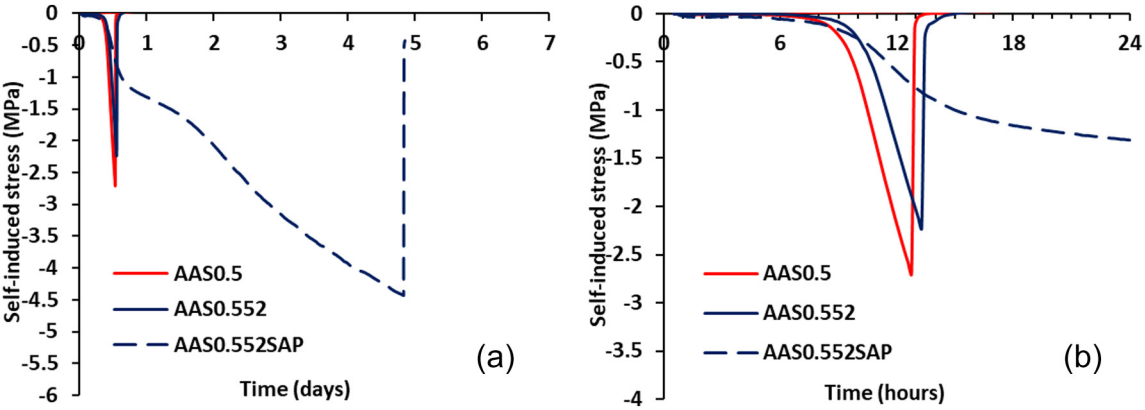

Fig. 7. Autogenous shrinkage-induced stress in AAS0.5, AAS0.552 and AAS0.552SAP (a), with the first 24 h amplified in (b).

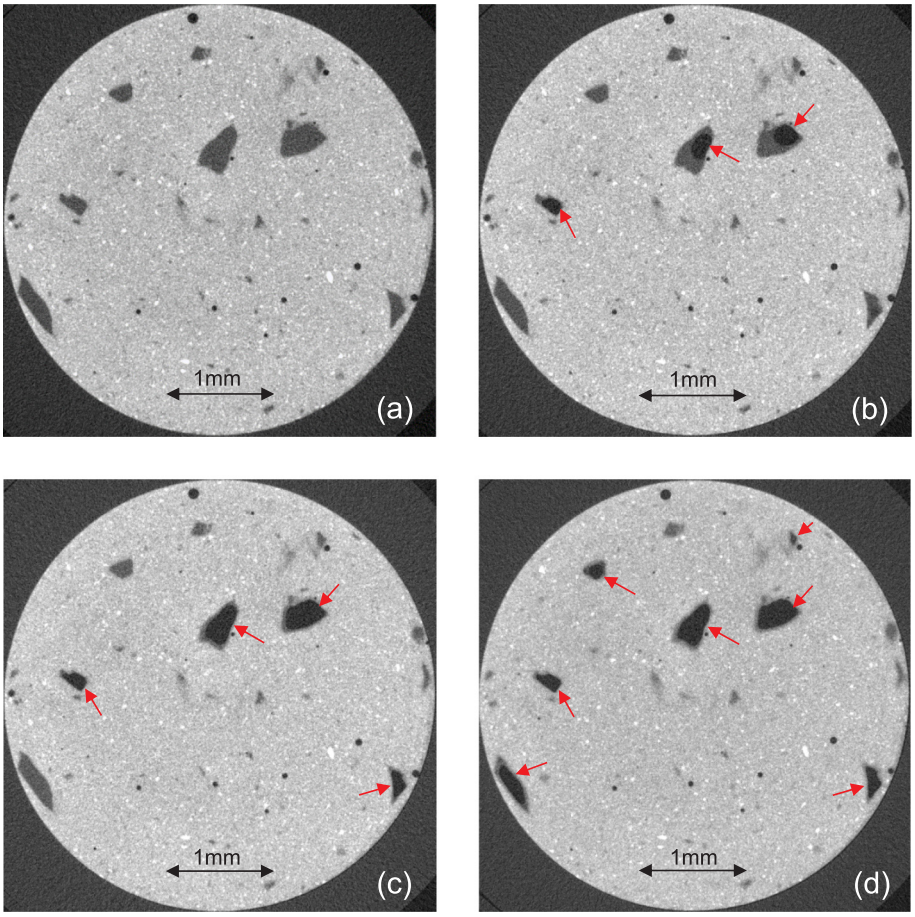

Fig. 8. A representative cross-section of AAS0.552SAP paste obtained by X-ray micro-tomography at the curing age of (a) 1 h, (b) 8 h, (c) 1 day and (d) 7 days. Several phases can be distinguished within the paste (light grey) including unreacted slag particles (white), SAP with liquid (dark grey), entrapped air (black and spherical) and the newly formed voids (black, marked by the arrows) within the SAP cavities.

indicating more liquid is released from the SAP. At the age of 7 days, most of the SAP located at the chosen cross-section have been emptied, while some of them still have liquid stored within, indicated by the dark grey color of these SAP-originated voids. This part of liquid may be useful for further reaction after 7 days. At the given resolution, no reaction products forming inside the SAP voids could be identified.

3.8. Mechanical properties

The compressive strength of the mixtures is shown in Fig. 9. In general, the compressive strength decreases with increased l/b and the reduction is more significant for pastes with increased l/b plus SAP. The difference in the compressive strength between the pastes with and without SAP does not decrease in time up to 6 days of age.

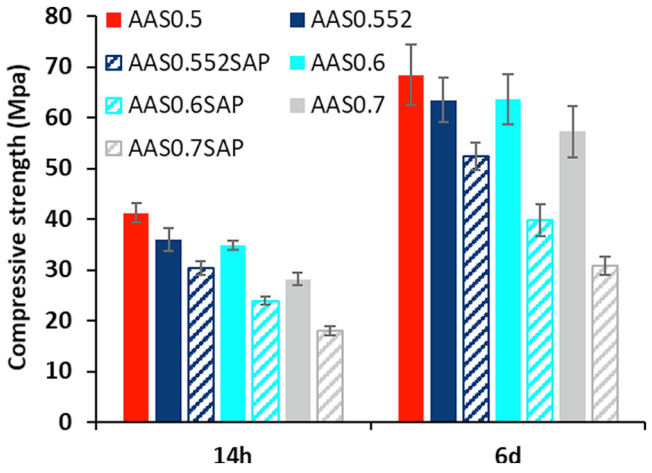

Fig. 9. Compressive strength of AAS pastes.

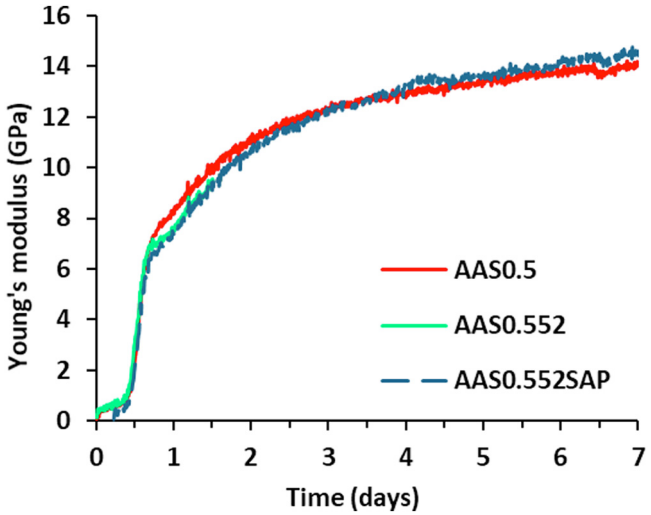

Fig. 10. Young's modulus of AAS pastes.

Fig. 10 shows the Young's modulus development of AAS0.5, AAS0.552, and AAS0.552SAP. The Young's modulus of the paste varies in the range of 0–0.5 GPa in the first 8–9 h before it increase rapidly. The Young's modulus of AAS0.5 and AAS0.552SAP were similar in the whole period studied. AAS0.552 showed similar evolution with the other mixtures in the first 1.5 days, after which the evolution stopped, most likely due to cracking of the paste or delamination of the paste from the test tube caused by the shrinkage.

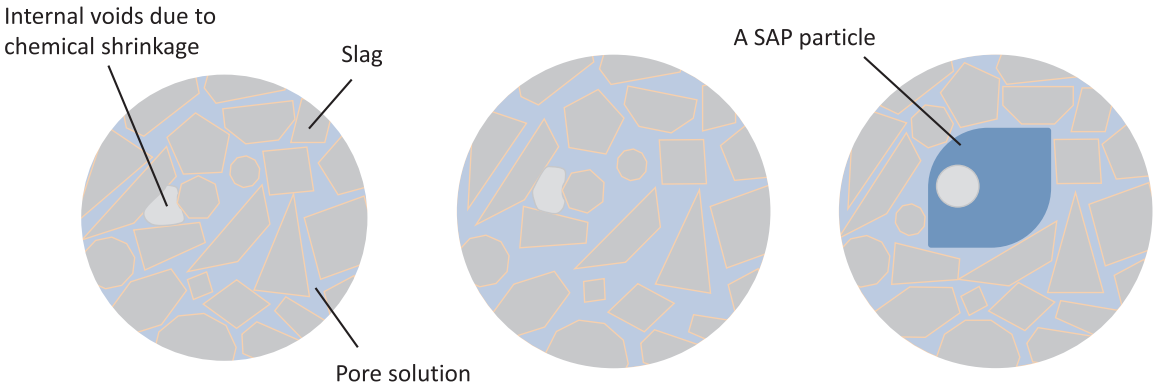

Fig. 11.

4. Discussion

4.1. Liquid absorption and release of SAP

According to Fig. 2, the SAP absorb the most in deionized water and the least in the activator. This is consistent with the lower absorption capacity of SAP in cement filtrate solution compared to deionized water [51], since different ions concentrations result in different osmotic pressures of the solution. The absorption capacity of SAP in water, 200 g/g at 24 h, is comparable with the data reported in the literature for similar types of SAP [30]. In NaOH solution, in contrast, there are large amounts of Na^+ and OH^-, which lead to screening of the repulsive interactions between charged groups within the polymer network and thus reduce the osmotic pressure. Therefore, the SAP absorb much less NaOH solution than deionized water.

Compared with the pure NaOH solution, the activator contains the same amount of Na^+, but part of the OH^- is substituted by SiO_3^{2-}. According to [52–54], divalent ions (e.g. Ca^{2+} and SO_4^{2-}) have stronger interactions with polyacrylamide-based gels and can better screen the charges of SAP than monovalent ions (e.g. Na^+, K^+, OH^- and NO_3^-). As a result, the repulsive force is reduced due to this electrostatic screening and hence the SAP experience lower swelling. Although no data is available in the literature, a similar enhanced screening effect may be expected for the divalent SiO_3^{2-} ions present in the activator. Besides SiO_3^{2-}, part of Si in the activator exists as monomer (SiO_2 or $Si(OH)_4$) or even oligomers [55,56], which may also contribute to a reduced absorption capacity of SAP in solution. However, the influence of these species on the absorption capacity of the SAP is not known yet.

Besides the absorption capacity, the influence of SAP on the ions concentrations in the alkali solution also needs to be considered. For alkali-activated materials, the reaction kinetics and the microstructure development largely depend on the ions concentrations in the pore solution. If the SAP preferentially absorbed water or ions, the concentration of the ions in the pore solution would be affected. For example, the SAP used in [57] was found to release Na^+ and OH^- and affect the hydration kinetics. As shown in Fig. 3, the ions concentrations in the activator decrease slightly (up to 4%) after absorption by SAP for 24 h. However, the magnitude of the change was amplified by the artificially high amount of SAP in the liquid necessary to resolve the possible changes. In the real paste, the amount of solution is considerably higher (only about 10% of the solution is absorbed in the paste with 0.552 l/b), hence the changes in the concentration of ions would be about 4 times less significant, likely below 1%. This indicates that the internal curing by SAP influences the paste mainly by providing extra activator rather than affecting the initial ions concentrations of the pore solution. This information is helpful to understand the reaction kinetics of the internally cured mixtures, which will be discussed in detail in the next section.

The SAP start to release liquid in the initial hours (before 8 h from mixing) as indicated by the X-ray tomography results. The SAP particles are emptied from the inside, which is consistent with the phenomenon observed in SAP-containing OPC based systems [58]. What is different is that not much reaction product is formed within the voids left by SAP in the AAS system in the first week of curing, as indicated in Figs. 8 and 9. In OPC systems, reaction products, especially portlandite, can even fill the voids left by the SAP (e.g., see Fig. 2 of [29]). In AAS systems, in contrast, amorphous C-A-S-H gels, which are the main reaction products, do not usually grow in large voids. Nonetheless, it is not excluded that a layer of reaction products can form at the original interface between SAP particles and the paste, which cannot be clearly distinguished at the current resolution. As long as the effectiveness of SAP in OPC based systems is well known (e.g., [27,29,54,58–60]), here we demonstrated with X-ray microtomography the absorption and desorption behavior of SAP in the AAS system.

4.2. Reaction kinetics and setting

The initial reaction rate of the paste is critically influenced by the alkalinity of the activator, which controls the dissolution of the slag [61]. Since the composition of the activator was kept constant with different l/b and the absorption of SAP does not significantly change the ions concentration of the surrounding solution, the heat flow and the total heat release in the initial hours of different mixtures are rather similar (Fig. 4). The main heat flow peak indicates the formation of the majority of the reaction products, i.e. C-A-S-H gels, from the ions in the activator and new ions dissolved from the slag. The l/b and the presence of SAP have major influences on the reaction in this stage. To explain the influences better, a schematic diagram on the pore structure of pastes with and without SAPs is shown in Fig. 11.

For the pastes without SAP, the activator distributes evenly in the interstitial space. At higher liquid content, the space between the slag particles is enlarged (comparing Fig. 11(a) and (b)) and more silicates and alkali ions are available in the pore solution. Hence, more ions such as Ca^{2+} and Al^{3+} need to be dissolved from the slag to reach critical Al/Si and Ca/Si in the pore solution before the reaction rate reaches a peak. For this reason the heat flow peak appears later for mixtures with higher l/b without SAP. Due to the presence of a higher amount of ions at the heat peak, the amplitudes of the heat release peak becomes higher. Since the mixtures with higher l/b without SAP have larger initial interstitial porosity, a longer time is needed before the transport of ions can be inhibited. Therefore, the mixtures with higher l/b without SAP show longer acceleration periods, as indicated by the broader heat flow peaks (Fig. 4(a)). The higher amount of reactants

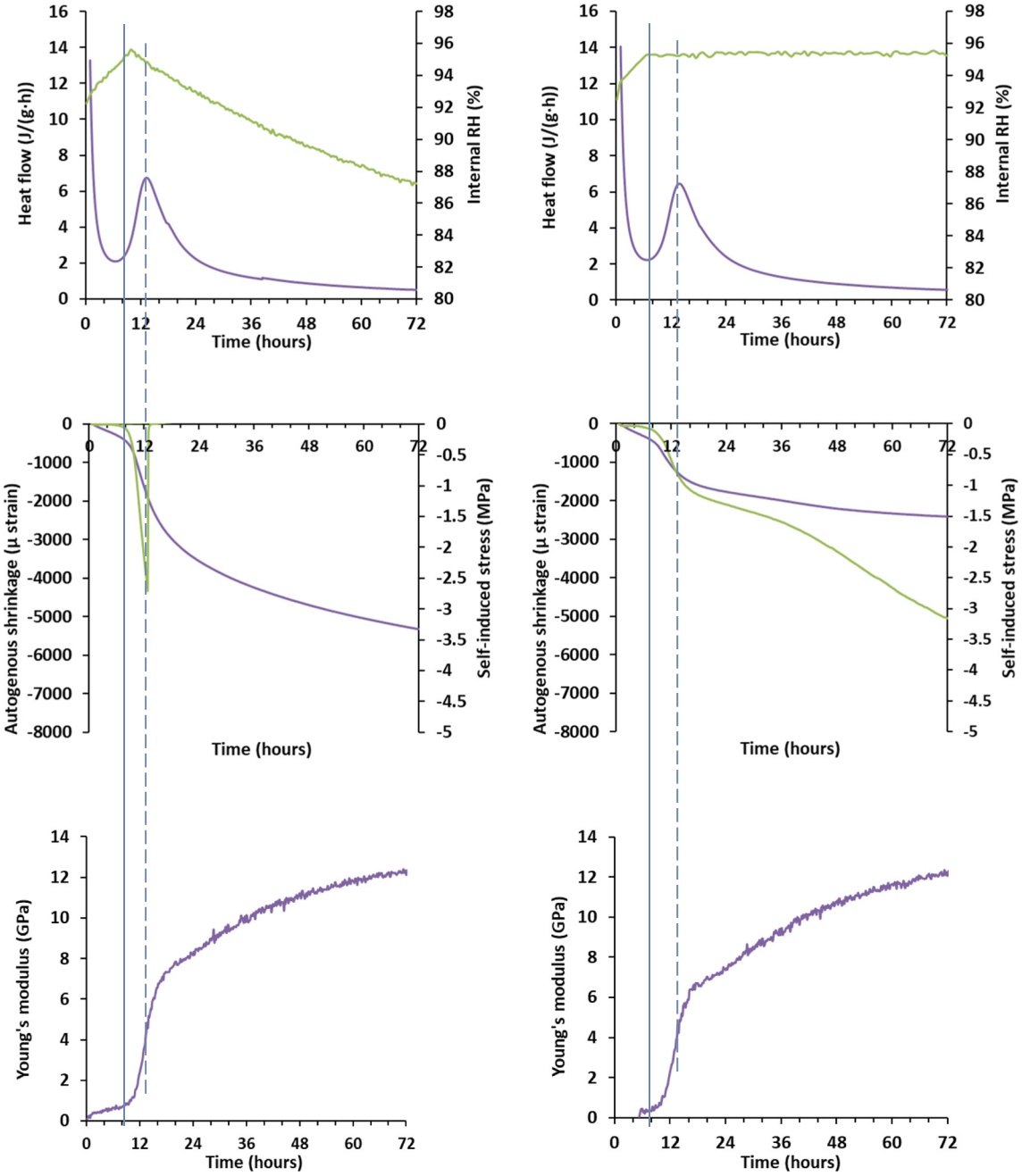

Fig. 12. Heat flow plotted together with internal RH, autogenous shrinkage, self-induced stress and Young's modulus of (left) AAS0.5 and (right) AAS0.552SAP. 0 h of all the curves represents the moment of adding liquid.

from the activator and the longer acceleration period contribute to the higher total heat release of mixtures with higher l/b without SAP (Fig. 4(b)). The delayed appearance of the main reaction peak and the increased total reaction degree of the paste with higher l/b are similar to what has been reported for OPC paste [63–65].

For the pastes with SAP, in contrast, extra activator is stored in the SAP particles before being released (comparing Fig. 11(a) and (c)). The ions in the SAP are therefore not instantaneously available for reactions with the slag compared to the ions in the interstitial space [63]. The activator gradually released from the SAP, on one hand, provides more reactants to the adjacent paste, and on the other hand, dilutes the concentrations of Ca^{2+} and Al^{3+} that are dissolved from slag. The reaching of critical Ca/Si and Al/Si through which the C-A-S-H gels can rapidly form is therefore buffered. Hence, compared to the control mixture AAS0.5 with the same l/b as the basic l/b in the paste with SAP, the start of the acceleration period is a bit delayed and the magnitude of the peak reaction rates is slightly lowered (Fig. 4(a)). Nonetheless, the buffering effect decreases as the activator is continuously released from the SAP. Due to the eventually higher activator content of SAP-containing mixtures than in the AAS0.5 control mixture, the total reaction degrees are higher after 24 h of curing, as indicated in Fig. 4(b).

Compared with the mixtures with the same liquid content but without SAP, SAP-containing pastes have the same initial total porosity, but different pore size distribution. Since a large amount of liquid is stored in the SAP, internally cured mixtures have, besides the macro voids induced by the SAP, lower interstitial pore space among the slag particles (comparing Fig. 11(b) and (c)). The lower interstitial pore space means a smaller space for the formation of reaction products around slag particles and thus a faster solid-phase percolation. After a large amount of reaction products is formed in the interstitial space, the

further dissolution of slag and the transport of ions would be inhibited (see the dense microstructure of AAS paste in Fig. 9 in this study and Fig. 4.20 in [66]). Therefore, the reaction rate of SAP-containing paste is slower than in the paste with the same total l/b but without SAP, especially after the acceleration period. The smaller amount of activator that is instantaneously available for the reaction and the limited interstitial space for transport and formation of reaction products induce a lower reaction rate after the acceleration period and thus a lower total reaction degree of internally cured mixtures compared to the mixtures with the same l/b but without SAP.

The times of initial and final set of the pastes are also delayed for mixtures with higher l/b. However, it should be noted that the delay in setting time is not associated with the delayed heat flow peak, since set of the AAS pastes happened much earlier than the beginning of the acceleration period. This phenomenon is different from what has been observed in OPC, for which final set normally happens at the beginning of the acceleration period [65]. In OPC, setting is a consequence of the percolation of the solid microstructure resulting from the continuous formation of reaction products surrounding the cement particles. In AAS, however, the pore solution contains besides water plenty of silicate ions, which act as not only reactants but also nuclei where reaction products can form [67]. The direct formation of reaction products in the interstitial space plus the high space-filling effect of the main products, C-A-S-H gels, result in a much easier and faster formation of initial network in AAS paste than in OPC [68]. This is the reason why slag-based alkali-activated materials normally show fast setting [69], which is much in advance of the beginning of the acceleration period. In the setting mechanism, the basic l/b plays a more important role since it determines the initial interstitial porosity of the paste. A finer interstitial porosity between slag particles ensures a shorter distance for the diffusion of Ca^{2+} and Al^{3+} from slag to form reaction products that can fill the space. Although internally cured mixtures contain large voids initially occupied by SAP, these voids seem to matter much less than the interstitial pores for the setting of the paste. For internally cured pastes, the basic l/b is similar to the control mixture, so the initial setting time of AAS0.552SAP and AAS0.6SAP are quite close to that of AAS0.5. This phenomenon is consistent with the finding for internally cured OPC pastes [29]. For the pastes without SAP, however, the time of final set increases significantly with increased l/b. The delay of setting by internal curing is beneficial to AAS systems, which are known to set too fast, but this beneficial delay comes at the expense of a loss in compressive strength, as shown in Fig. 9.

4.3. Internal RH, autogenous shrinkage and self-induced stress

By plotting together the curves of reaction heat, internal RH, autogenous shrinkage, Young's modulus and self-induced stress of AAS0.5 and AAS0.552SAP, it can be seen that these parameters develop following the same kinetics, as shown in Fig. 12. The evolution of the autogenous shrinkage of AAS can be approximately divided into three stages: dormant period (0–9 h), acceleration period (9–24 h) and late period (after 24 h).

4.3.1. Stage I: Dormant period

In the first 8–9 h (indicated by the solid line in Fig. 12), the reactions are mainly in the dormant period indicated by the reaction heat. In this stage, the RH of the pastes experiences an increase most likely due to the consumption of the ions from the activator [37]. In fact, internal voids in the paste should have started to form in this period, which would result in the buildup of initial pore pressure; otherwise, the liquid in the SAP in AAS0.552SAP would not be consumed as shown in Fig. 8(b). Therefore, the RH_K of the paste without SAP should have decreased. A relatively low suction would be necessary to remove activator from the large SAP voids. Because only the largest pores are emptied, very low pore pressure develops. Thus, the decrease of internal RH resulting from the presence of menisci is not evident and is probably overcome by the RH increase due to ions concentration decrease; thus, the paste experiences an increase of overall RH in this stage.

In this period, due to the slow development of the Young's modulus, the self-induced stresses of the mixtures remain close to zero, despite the fact that the autogenous shrinkage of AAS0.5 and AAS0.552SAP reaches 460 μm/m and 455 μm/m at 8 h, respectively, as shown in Fig. 12. As indicated by the low Young's modulus of the pastes, the non-decreasing internal RH and the limited shrinkage-induced stress, the autogenous shrinkage in this period appears to be mainly viscous or even plastic deformation rather than elastic deformation under a considerable pore pressure. The similar autogenous shrinkage values of AAS0.552SAP and AAS0.5 during this early period confirm this hypothesis.

From this aspect, it becomes arguable if the time of final set determined by the Vicat method should be chosen as the “time-zero” for the autogenous shrinkage of sodium silicate activated slag systems like for OPC. As discussed in Section 4.2, the time of final set of OPC normally indicates the formation of solid percolation, when the reaction products surrounding the cement particles start forming a solid cluster that spans the whole sample [65]. In sodium silicate activated slag system, in contrast, the time of final set is probably the result of flowability loss of the paste due to the formation of initial products in the interstitial space based on alkali and silicate ions in the activator [70]. At such a short time (around half an hour after mixing), a solid skeleton with enough stiffness has not formed yet. The Young's modulus measurements also confirm this hypothesis, as no rapid increase is observed around the Vicat setting time. From the cracking potential point of view, the time when the paste starts to generate internal stress under restrained condition, around 8 h in the case of this study, seems a better definition of the “time-zero” of the autogenous shrinkage. This “time-zero” is just the time instant when the acceleration period begins, when the autogenous shrinkage developing rate increases, and also when the internal RH starts to decrease, as shown in Fig. 12. If the autogenous shrinkage of AAS is zeroed at 7 or 8 h, the total curve would be around 460 μm lower than shown in Fig. 12. Nonetheless, it is noticed that the autogenous shrinkage of AAS pastes is still much higher than normal OPC pastes if internal curing is not applied.

4.3.2. Stage II: Acceleration period

About 8–9 h after mixing, the heat flow rates of the pastes increase rapidly, which indicates the formation of large amounts of reaction products. In this acceleration period, the RH of the pastes starts to drop, indicating the rapid formation of internal voids and fast development of pore pressure. As a result, the autogenous shrinkage of AAS0.5 starts to develop at a high speed, as shown in Fig. 12. In addition, a rapid evolution of the Young's modulus was observed from this time instant on. The rapid evolution of autogenous shrinkage in the mixture without SAP together with the rapid evolution of stiffness are responsible for the corresponding fast evolution of restraint stresses and eventually for the cracking. Considering the higher compressive strength of the AAS0.5 paste compared to the AAS0.552SAP paste (see Fig. 9), a higher tensile strength can also be expected. This could explain the higher stress at cracking of the AAS0.5 paste. With the help of internal curing by SAP, mixture AAS0.552SAP keeps a high level of internal RH, and the autogenous shrinkage and restraint stress develop at low rates. The similar stiffness of AAS0.5 and AAS0.552SAP confirms that the lower stress generated in restrained AAS0.5 is due to the reduced autogenous shrinkage rather than a lowered Young's modulus.

As shown by the RH results, the SAP content of 0.26%, chosen based on the chemical shrinkage of the paste and the absorption capacity of SAP can already provide nearly saturated conditions to the paste in the period studied. This is consistent with the X-ray tomography results shown in Fig. 8. This explains why higher SAP contents did not have much further mitigation effect on the autogenous shrinkage (see Fig. 6).

While internal curing successfully mitigated more than half of the

autogenous shrinkage in this period, a part of autogenous shrinkage of AAS remains when SAP is present, even at higher dosages along with a sufficient amount of additional liquid. As shown in Fig. 12, the autogenous shrinkage of AAS0.552SAP keeps increasing when the RH_K is nearly 100%, although the developing rate is lower than that of both AAS0.5 and AAS0.052. The continuous developments of autogenous shrinkage of AAS0.552SAP results in the slow but continuous increase of the self-induced stress, which eventually leads to cracking of the paste at about 5 days. Such a development of autogenous shrinkage under nearly saturated conditions was not observed in OPC based systems. Those systems would show zero shrinkage or even expansion when enough internal curing water were provided [28,71]. This indicates that besides self-desiccation, there may be other mechanisms causing autogenous shrinkage in AAS, especially in the acceleration period. Further studies are needed to determine the driving force of the autogenous shrinkage component that cannot be mitigated by internal curing.

4.3.3. Stage III: After 24 h

After the main reaction peak, the reaction rates reduce and so do the rates of autogenous shrinkage in AAS0.5 and AASF0.552SAP. Chemical shrinkage and self-desiccation still develop in AAS0.5, as indicated by the continuous RH decrease (Fig. 12). At the same time, the liquid is continuously released from the SAP in mixture AAS0.552SAP between 1 and 7 days to compensate for the chemical shrinkage as shown in Fig. 8(c) and (d). These indicate that the pore pressure becomes the predominant driving force of the autogenous shrinkage of AAS paste in this period.

4.4. Mechanical properties

Fig. 10 shows that the compressive strength is decreased with increased l/b. These phenomena are generally in line with what has been observed in OPC since higher l/b normally means higher porosity and therefore lower compressive strength [29,72,73]. The presence of SAP decreases the compressive strength further due to the incorporation of macro-level voids. At later times, the difference in the compressive strength between mixtures with higher l/b without SAP and control mixture decreases, while the difference between the SAP-containing mixtures and control mixture does not. This is because the larger interstitial spaces in mixtures with higher l/b without SAP can be more easily filled by reaction products compared to the larger voids induced by SAP. With the reaction going on, the microstructure of pastes with higher l/b without SAP would become eventually dense enough to at least partially compensate the strength loss, but the SAP-originated voids will mostly remain as defects, as shown in Fig. 8 and Fig. 9. This analysis has been confirmed by the higher total reaction heat of non-SAP samples than SAP-containing samples with the same l/b (Fig. 4).

While the compressive strength of the paste is decreased by internal curing, the Young's modulus of the paste seems not. This is most likely because strength is more sensitive to large voids (defects) originating from the swollen SAP. A further reason might be that the SAP limited microcracking in the pastes and its negative effect primarily on the Young's modulus [74].

Considering the detrimental impact on the compressive strength of internal curing and the limited mitigation of autogenous shrinkage by higher contents of SAP, it seems that the dosage determined based on chemical shrinkage is the optimal dosage to provide internal curing to AAS paste and further increasing the dosage would not have any significant positive effect.

5. Conclusions

In this study, the absorption and desorption behavior of SAP in AAS systems was studied and the mechanism of the mitigating effect on autogenous shrinkage of AAS was clarified. The influence of SAP incorporation on the mechanical properties of AAS pastes was also studied. Following remarks can be made based on this study:

1. The SAP show a significantly lower absorption capacity in alkali activator than in water, and still lower than in pure NaOH solution. Even though there exists a slight absorption preference for ions over water from the activator, it is of negligible importance for the small amounts of SAP compared to liquid applied in the pastes. In the internally cured sample, the SAP are observed to release liquid to the surrounding paste starting from before 8 h. After the first week, there is still a certain amount of liquid left in the SAP for mixture AAS0.552SAP, indicating a further internal curing potential for later reactions. In the period studied, there is a negligible amount of reaction products filling the SAP voids.
2. Internal curing by SAP prolongs the time of final set and the time at which the peak of reaction heat occurs, but it increases the total reaction degree of AAS pastes at longer term due to the higher content of activator. Compared to the mixtures with the same liquid amount but without SAP, internally cured mixtures show lower reaction degrees due to the smaller interstitial space for the formation of reaction products.
3. Internal curing by SAP can largely reduce the autogenous shrinkage and cracking tendency of AAS. This is beneficial to tackle the problem of large autogenous shrinkage of AAS in practical applications. Nonetheless, part of the autogenous shrinkage cannot be eliminated, regardless of the amounts of SAP, especially in the acceleration period. This suggests the existence of other causes of autogenous shrinkage besides self-desiccation.
4. While the addition of SAP only slightly influenced the Young's modulus of AAS paste, it can largely decrease the compressive strength of AAS paste.
5. Designing the SAP content from the chemical shrinkage of the paste and the absorption capacity of SAP measured by the teabag method yields the optimal dosage in terms of shrinkage mitigation, while guarantying limited negative effects on strength. Therefore, this procedure is recommended for future applications. For the particular SAP used in our study with absorption capacity of the activator of 20 g/g, this procedure corresponded to 0.26% (by mass of slag precursor).

CRediT authorship contribution statement

Zhenming Li: Conceptualization, Methodology, Investigation, Writing - original draft. **Mateusz Wyrzykowski:** Conceptualization, Methodology, Supervision, Writing - review & editing. **Hua Dong:** Methodology. **José Granja:** Methodology. **Miguel Azenha:** Methodology. **Pietro Lura:** Conceptualization, Methodology, Supervision, Writing - review & editing. **Guang Ye:** Conceptualization, Supervision, Writing - review & editing.

Declaration of competing interest

The authors declare that they have no conflict of interest.

Acknowledgment

The funding supported by China Scholarship Council under grand number 201506120072 and by Netherlands Organisation for Scientific Research (NWO) are acknowledged. The short visit at Empa by the first author was supported by the STSM project “Towards the next generation of standards for the service life of cement-based materials and structures” of COST Action TU1404.

The funding provided by the Portuguese Foundation for Science and Technology (FCT) to the Research Project IntegraCrete (PTDC/ECM-EST/1056/2014 - POCI-01-0145-FEDER-016841) is gratefully

acknowledged, as well as the grant UID/ECI/04029/2019 - ISISE, funded by national funds through the FCT/MCTES (PIDDAC).

Mr. Janis Justs, Mr. Nikolajs Toropovs, Mr. Peihua Zhong and Dr. Zhangli Hu (all from Empa) are sincerely acknowledged for their help on the experiments performed in Empa and the discussions on the results.

References

[1] J.L. Provis, Alkali-activated materials, Cem. Concr. Res. 114 (2018) 40–48, https://doi.org/10.1016/j.cemconres.2017.02.009.
[2] R.J. Thomas, H. Ye, A. Radlinska, S. Peethamparan, Alkali-activated slag cement concrete, Concr. Int. 38 (2016) 33–38.
[3] P. Duxson, J.L. Provis, G.C. Lukey, J.S.J. van Deventer, The role of inorganic polymer technology in the development of “green concrete,”, Cem. Concr. Res. 37 (2007) 1590–1597, https://doi.org/10.1016/j.cemconres.2007.08.018.
[4] C. Shi, A.F. Jiménez, A. Palomo, New cements for the 21st century: the pursuit of an alternative to Portland cement, Cem. Concr. Res. 41 (2011) 750–763, https://doi.org/10.1016/j.cemconres.2011.03.016.
[5] J.L. Provis, J.S.J. Van Deventer, Geopolymers: Structures, Processing, Properties and Industrial Applications, Woodhead, Cambridge, UK, 2009.
[6] K. Arbi, M. Nedeljković, Y. Zuo, G. Ye, A review on the durability of alkali-activated fly ash/slag systems: advances, issues, and perspectives, Ind. Eng. Chem. Res. 55 (2016) 5439–5453, https://doi.org/10.1021/acs.iecr.6b00559.
[7] M.C.G. Juenger, F. Winnefeld, J.L. Provis, J.H. Ideker, Advances in alternative cementitious binders, Cem. Concr. Res. 41 (2011) 1232–1243, https://doi.org/10.1016/j.cemconres.2010.11.012.
[8] S. Wang, X. Pu, K.L. Scrivener, P.L. Pratt, Alkali-activated slag cement and concrete: a review of properties and problems, Adv. Cem. Res. 7 (1995) 93–102, https://doi.org/10.1680/adcr.1995.7.27.93.
[9] Z. Li, J. Liu, G. Ye, Drying shrinkage of alkali-activated slag and fly ash concrete. A comparative study with ordinary Portland cement concrete, Proc. Work. Concr. Model. Mater. Behav. Honor Profr. Klaas van Breugel, Delft, 2018, pp. 160–166.
[10] Z. Li, M. Nedeljkovic, Y. Zuo, G. Ye, Autogenous shrinkage of alkali-activated slag-fly ash pastes, 5th Int. Slag Valoris. Symp., Leuven, 2017, pp. 369–372.
[11] Z. Li, A. Kostiuchenko, G. Ye, Autogenous shrinkage-induced stress of alkali-activated slag and fly ash concrete under restraint condition, in: ECI (Ed.), Alkali Act. Mater. Geopolymers Versatile Mater. Offer. High Perform. Low Emiss., Tomar, 2018, p. 24.
[12] M. Palacios, F. Puertas, Effect of shrinkage-reducing admixtures on the properties of alkali-activated slag mortars and pastes, Cem. Concr. Res. 37 (2007) 691–702.
[13] A.R. Sakulich, D.P. Bentz, Mitigation of autogenous shrinkage in alkali activated slag mortars by internal curing, Mater. Struct. 46 (2013) 1355–1367, https://doi.org/10.1617/s11527-012-9978-z.
[14] H. Ye, A. Radlińska, Shrinkage mechanisms of alkali-activated slag, Cem. Concr. Res. 88 (2016) 126–135, https://doi.org/10.1016/j.cemconres.2016.07.001.
[15] H. Ye, A. Radlińska, Shrinkage mitigation strategies in alkali-activated slag, Cem. Concr. Res. 101 (2017) 131–143, https://doi.org/10.1016/j.cemconres.2017.08.025.
[16] B.D. Kumarappa, S. Peethamparan, M. Ngami, Autogenous shrinkage of alkali activated slag mortars: basic mechanisms and mitigation methods, Cem. Concr. Res. 109 (2018) 1–9, https://doi.org/10.1016/j.cemconres.2018.04.004.
[17] S. Oh, Y.C. Choi, Superabsorbent polymers as internal curing agents in alkali activated slag mortars, Constr. Build. Mater. 159 (2018) 1–8, https://doi.org/10.1016/j.conbuildmat.2017.10.121.
[18] C. Song, Y.C. Choi, S. Choi, Effect of internal curing by superabsorbent polymers – internal relative humidity and autogenous shrinkage of alkali-activated slag mortars, Constr. Build. Mater. 123 (2016) 198–206, https://doi.org/10.1016/j.conbuildmat.2016.07.007.
[19] V. Bílek, L. Kalina, R. Novotný, Polyethylene glycol molecular weight as an important parameter affecting drying shrinkage and hydration of alkali-activated slag mortars and pastes, Constr. Build. Mater. 166 (2018) 564–571, https://doi.org/10.1016/j.conbuildmat.2018.01.176.
[20] M. Criado, A. Palomo, A. Fernández-Jiménez, P.F.G. Banfill, Alkali activated fly ash: effect of admixtures on paste rheology, Rheol. Acta 48 (2009) 447–455, https://doi.org/10.1007/s00397-008-0345-5.
[21] G. Habert, J.B.D. De Lacaillerie, N. Roussel, An environmental evaluation of geopolymer based concrete production: reviewing current research trends, J. Clean. Prod. 19 (2011) 1229–1238.
[22] C.A. Rees, J.L. Provis, G.C. Lukey, J.S.J. van Deventer, The mechanism of geopolymer gel formation investigated through seeded nucleation, Colloids Surfaces A Physicochem. Eng. Asp. 318 (2008) 97–105, https://doi.org/10.1016/j.colsurfa.2007.12.019.
[23] M. Collepardi, A. Borsoi, S. Collepardi, J.J.O. Olagot, R. Troli, Effects of shrinkage reducing admixture in shrinkage compensating concrete under non-wet curing conditions, Cem. Concr. Compos. 27 (2005) 704–708.
[24] T. Bakharev, J.G. Sanjayan, Y. Cheng, Effect of elevated temperature curing on properties of alkali-activated slag concrete, Cem. Concr. Res. 29 (1999) 1619–1625.
[25] W. Tu, Y. Zhu, G. Fang, X. Wang, M. Zhang, Internal curing of alkali-activated fly ash-slag pastes using superabsorbent polymer, Cem. Concr. Res. 116 (2019) 179–190, https://doi.org/10.1016/j.cemconres.2018.11.018.
[26] V. Mechtcherine, M. Gorges, C. Schroefl, A. Assmann, W. Brameshuber, A.B. Ribeiro, D. Cusson, J. Custódio, E.F. Da Silva, K. Ichimiya, S.I. Igarashi, A. Klemm, K. Kovler, A.N. De Mendonça Lopes, P. Lura, V.T. Nguyen, H.W. Reinhardt, R.D.T. Filho, J. Weiss, M. Wyrzykowski, G. Ye, S. Zhutovsky, Effect of internal curing by using superabsorbent polymers (SAP) on autogenous shrinkage and other properties of a high-performance fine-grained concrete: results of a RILEM round-robin test, Mater. Struct. 47 (2014) 541–562, https://doi.org/10.1617/s11527-013-0078-5.
[27] O.M. Jensen, P.F. Hansen, Water-entrained cement-based materials - I. Principles and theoretical background, Cem. Concr. Res. 31 (2001) 647–654, https://doi.org/10.1016/S0008-8846(01)00463-X.
[28] P. Lura, F. Durand, O.M. Jensen, Autogenous strain of cement pastes with superabsorbent polymers, Proc. Internaltional RILEM Conf. Vol. Chang. Hardening Concr. Test. Mitig. C, 2006, pp. 57–66, , https://doi.org/10.1617/2351580052.007.
[29] J. Justs, M. Wyrzykowski, D. Bajare, P. Lura, Internal curing by superabsorbent polymers in ultra-high performance concrete, Cem. Concr. Res. 76 (2015) 82–90, https://doi.org/10.1016/j.cemconres.2015.05.005.
[30] D. Snoeck, O.M. Jensen, N. De Belie, The influence of superabsorbent polymers on the autogenous shrinkage properties of cement pastes with supplementary cementitious materials, Cem. Concr. Res. 74 (2015) 59–67, https://doi.org/10.1016/j.cemconres.2015.03.020.
[31] M. Wyrzykowski, P. Lura, Reduction of autogenous shrinkage in OPC and BFSC pastes with internal curing, Proc. XIII Int. Conf. Durab. Build. Mater. Components, São Paulo, Brazil, 2014, pp. 2–5.
[32] D. Snoeck, C. Schröfl, V. Mechtcherine, Recommendation of RILEM TC 260-RSC: testing sorption by superabsorbent polymers (SAP) prior to implementation in cement-based materials, Mater. Struct. 51 (2018) 116, https://doi.org/10.1617/s11527-018-1242-8.
[33] V. Mechtcherine, D. Snoeck, C. Schröfl, N. De Belie, A.J. Klemm, K. Ichimiya, J. Moon, M. Wyrzykowski, P. Lura, N. Toropovs, A. Assmann, S. ichi Igarashi, I. De La Varga, F.C.R. Almeida, K. Erk, A.B. Ribeiro, J. Custódio, H.W. Reinhardt, V. Falikman, Testing superabsorbent polymer (SAP) sorption properties prior to implementation in concrete: results of a RILEM Round-Robin Test, Mater. Struct. 51 (2018), https://doi.org/10.1617/s11527-018-1149-4.
[34] O.M. Jensen, Water absorption of superabsorbent polymers in a cementitious environment, Int. RILEM Conf. Adv. Constr. Mater. Through Sci. Eng, 2011, pp. 22–35.
[35] M. Wyrzykowski, S.-I. Igarashi, P. Lura, V. Mechtcherine, Recommendation of RILEM TC 260-RSC: using superabsorbent polymers (SAP) to mitigate autogenous shrinkage, Mater. Struct. 51 (2018) 135, https://doi.org/10.1617/s11527-018-1241-9.
[36] Z. Li, M. Nedeljković, B. Chen, G. Ye, Mitigating the autogenous shrinkage of alkali-activated slag by metakaolin, Cem. Concr. Res. 122 (2019) 30–41, https://doi.org/10.1016/j.cemconres.2019.04.016.
[37] Y. Zuo, M. Nedeljković, G. Ye, Pore solution composition of alkali-activated slag/fly ash pastes, Cem. Concr. Res. 115 (2019) 230–250, https://doi.org/10.1016/j.cemconres.2018.10.010.
[38] ASTM C 1608, Standard Test Method for Chemical Shrinkage of Hydraulic Cement Paste, (2007), pp. 667–670.
[39] Z. Li, S. Zhang, Y. Zuo, W. Chen, G. Ye, Chemical deformation of metakaolin based geopolymer, Cem. Concr. Res. 120 (2019) 108–118, https://doi.org/10.1016/j.cemconres.2019.03.017.
[40] NEN-EN 1097-7, Tests for Mechanical and Physical Properties of Aggregates - Part 7: Determination of the Particle Density of Filler - Pyknometer Method, (2008), pp. 1–13.
[41] P. Lura, O.M. Jensen, K. Van Breugel, Autogenous shrinkage in high-performance cement paste: an evaluation of basic mechanisms, Cem. Concr. Res. 33 (2003) 223–232, https://doi.org/10.1016/S0008-8846(02)00890-6.
[42] ASTM C1968, Standard Test Method for Autogenous Strain of Cement Paste and Mortar, (2013), pp. 1–8, https://doi.org/10.1520/C1698-09.2.
[43] M. Wyrzykowski, Z. Hu, S. Ghourchian, K. Scrivener, P. Lura, Corrugated tube protocol for autogenous shrinkage measurements: review and statistical assessment, Mater. Struct. 50 (2017) 57, https://doi.org/10.1617/s11527-016-0933-2.
[44] M. Grzybowski, S.P. Shah, Shrinkage cracking of fiber reinforced concrete, Mater. J. 87 (1990) 138–148.
[45] K. Kovler, J. Sikuler, A. Bentur, Restrained shrinkage tests of fibre-reinforced concrete ring specimens: effect of core thermal expansion, Mater. Struct. 26 (1993) 231–237.
[46] J.L. Schlitter, A.H. Senter, D.P. Bentz, T. Nantung, W.J. Weiss, A dual concentric ring test for evaluating residual stress development due to restrained volume change, J. ASTM Int. 7 (2010) 1–13.
[47] NEN 196-1, Methods of Testing Cement–Part 1: Determination of Strength, 2005, Eur. Comm. Stand, 2005.
[48] M. Azenha, R. Faria, F. Magalhães, L. Ramos, Á. Cunha, Measurement of the E-modulus of cement pastes and mortars since casting, using a vibration based technique, Mater. Struct. 45 (2012) 81–92, https://doi.org/10.1617/s11527-011-9750-9.
[49] Z. Hu, M. Wyrzykowski, P. Lura, Estimation of reaction kinetics of geopolymers at early ages, Cem. Concr. Res. 129 (2020) 105971, , https://doi.org/10.1016/j.cemconres.2020.105971.
[50] O.M. Jensen, Autogenous Deformation and RH-change—Self-desiccation and Self-desiccation Shrinkage (in Danish), Phd Thesis, Build. Mater. Lab. Tech. Univ. Denmark, Lyngby, Denmark, 1993, p. 285.
[51] P. Zhong, M. Wyrzykowski, N. Toropovs, L. Li, J. Liu, P. Lura, Internal curing with superabsorbent polymers of different chemical structures, Cem. Concr. Res. 123 (2019) 105789, , https://doi.org/10.1016/j.cemconres.2019.105789.
[52] Q. Zhu, C.W. Barney, K.A. Erk, Effect of ionic crosslinking on the swelling and mechanical response of model superabsorbent polymer hydrogels for internally

cured concrete, Mater. Struct. 48 (2015) 2261–2276, https://doi.org/10.1617/s11527-014-0308-5.
[53] W. Siriwatwechakul, J. Siramont, W. Vichi-Vadakan, Superabsorbent Polymer Structures, Int. RILEM Conf. Use Superabsorbent Polym. Other New Addit. Concr, (2010), pp. 253–262.
[54] C. Schröfl, V. Mechtcherine, M. Gorges, Relation between the molecular structure and the efficiency of superabsorbent polymers (SAP) as concrete admixture to mitigate autogenous shrinkage, Cem. Concr. Res. 42 (2012) 865–873, https://doi.org/10.1016/j.cemconres.2012.03.011.
[55] A. Favier, G. Habert, N. Roussel, J.-B. d'Espinose de Lacaillerie, A multinuclear static NMR study of geopolymerisation, Cem. Concr. Res. 75 (2015) 104–109, https://doi.org/10.1016/j.cemconres.2015.03.003.
[56] J.L. Bass, G. Turner, Anion distributions in sodium silicate solutions. Characterization by ^{29}Si NMR and infrared spectroscopies, and vapor phase osmometry, J. Phys. Chem. B 101 (1997) 10638–10644, https://doi.org/10.1021/jp9715282.
[57] H.X.D. Lee, H.S. Wong, N.R. Buenfeld, Effect of alkalinity and calcium concentration of pore solution on the swelling and ionic exchange of superabsorbent polymers in cement paste, Cem. Concr. Compos. 88 (2018) 150–164.
[58] H. Lee, Potential of superabsorbent polymer for self-sealing cracks in concrete, Adv. Appl. Ceram. 109 (2009) 296–302, https://doi.org/10.1179/174367609x459559.
[59] M. Kamali, A. Ghahremaninezhad, An investigation into the influence of superabsorbent polymers on the properties of glass powder modified cement pastes, Constr. Build. Mater. 149 (2017) 236–247, https://doi.org/10.1016/j.conbuildmat.2017.04.125.
[60] J. Siramanont, W. Vichit-Vadakan, W. Siriwatwechakul, International RILEM Conference on Use of Superabsorbent Polymers and Other New Additives in Concrete The Impact of sap Structure on the Effectiveness of Internal Curing, (2010).
[61] C. Shi, R.L. Day, A calorimetric study of early hydration of alkali-slag cements, Cem. Concr. Res. 25 (1995) 1333–1346.
[62] D. Ravikumar, N. Neithalath, Reaction kinetics in sodium silicate powder and liquid activated slag binders evaluated using isothermal calorimetry, Thermochim. Acta 546 (2012) 32–43, https://doi.org/10.1016/j.tca.2012.07.010.
[63] J. Justs, M. Wyrzykowski, F. Winnefeld, D. Bajare, P. Lura, Influence of superabsorbent polymers on hydration of cement pastes with low water-to-binder ratio: a calorimetry study, J. Therm. Anal. Calorim. 115 (2014) 425–432, https://doi.org/10.1007/s10973-013-3359-x.
[64] T. Zhang, Q. Yu, J. Wei, P. Gao, P. Zhang, Study on optimization of hydration process of blended cement, J. Therm. Anal. Calorim. 107 (2011) 489–498.
[65] G. Ye, Experimental Study and Numerical Simulation of the Development of the Microstructure and Permeability of Cementitious Materials, (2003).
[66] M. Nedeljković, Carbonation Mechanism of Alkali-activated Fly Ash and Slag Materials: In View of Long-term Performance Predictions, Delft University of Technology, 2019.
[67] J.L. Provis, J.S.J. van Deventer, Geopolymerisation kinetics. 2. Reaction kinetic modelling, Chem. Eng. Sci. 62 (2007) 2318–2329, https://doi.org/10.1016/j.ces.2007.01.028.
[68] Y. Zuo, G. Ye, Pore Structure Characterization of Sodium Hydroxide Activated Slag Using Mercury Intrusion Porosimetry, Nitrogen Adsorption, and Image Analysis, (2018), https://doi.org/10.3390/ma11061035.
[69] M. Nedeljković, Z. Li, G. Ye, Setting, strength, and autogenous shrinkage of alkali-activated fly ash and slag pastes: effect of slag content, Materials (Basel) 11 (2018) 2121, https://doi.org/10.3390/ma11112121.
[70] A. Fernández-Jiménez, F. Puertas, et al., Effect of activator mix on the hydration and strength behaviour of alkali-activated slag cements, Adv. Cem. Res. 15 (2003) 129–136.
[71] O.M. Jensen, Use of superabsorbent polymers in construction materials, 1st Int. Conf. Microstruct. Relat. Durab. Cem. Compos, 2008, pp. 757–764 13–15 Oct.
[72] M.T. Hasholt, O.M. Jensen, K. Kovler, S. Zhutovsky, Can superabsorent polymers mitigate autogenous shrinkage of internally cured concrete without compromising the strength? Constr. Build. Mater. 31 (2012) 226–230.
[73] P. Lura, F. Durand, A. Loukili, K. Kovler, O.M. Jensen, Compressive strength of cement pastes and mortars with superabsorbent polymers, Proc. Int. RILEM Conf. Vol. Chang. Hardening Concr. Test. Mitig, 2006, pp. 117–125.
[74] F.C.S. Carvalho, C.-N. Chen, J.F. Labuz, Measurements of effective elastic modulus and microcrack density, Int. J. Rock Mech. Min. Sci. 34 (1997) (43–e1).